AMERICAN SOCIETY FOR MICROBIOLOGY | Infection and Immunity

Immunology | Full-Length Text

Phospholipase C epsilon-1 (PLCℰ1) mediates macrophage activation and protection against tuberculosis

Ananya Gupta,[1] Shyamala Thirunavukkarasu,[2] Javier Rangel-Moreno,[3] Mushtaq Ahmed,[1] Rosemary V. Swanson,[2] Stanley Kimbung Mbandi,[4] Alan V. Smrcka,[5] Deepak Kaushal,[6] Thomas J. Scriba,[4] Shabaana A. Khader[1]

AUTHOR AFFILIATIONS See affiliation list on p. 13.

ABSTRACT Tuberculosis (TB) caused by *Mycobacterium tuberculosis* (*Mtb*) infects up to a quarter of the world's population. Although immune responses can control *Mtb* infection, 5%–10% of infected individuals can progress to active TB disease (progressors). A myriad of host factors regulate disease progression in TB and a better understanding of immune correlates of protection and disease is pivotal for the development of new therapeutics. Comparison of human whole blood transcriptomic metadata with that of macaque TB progressors and *Mtb*-infected diversity outbred mice (DO) led to the identification of differentially regulated gene (DEG) signatures, associated with TB progression or control. The current study assessed the function of Phospholipase C epsilon (*PLCℰ1*), the top downregulated gene across species in TB progressors, using a gene-specific knockout mouse model of *Mtb* infection and in vitro *Mtb*-infected bone marrow-derived macrophages. *PLCℰ1* gene expression was downregulated in TB progressors across species. *PLCε1* deficiency in the mouse model resulted in increased susceptibility to *Mtb* infection, coincident accumulation of lung myeloid cells, and reduced ability to mount antibacterial responses. However, *PLCε1* was not required for the activation and accumulation of T cells in mice. Our results suggest an important early role for *PLCℰ1* in shaping innate immune response to TB and may represent a putative target for host-directed therapy.

KEYWORDS 1-phosphatidylinositol-4, 5-bisphosphate phosphodiesterase epsilon-1 (*PLCℰ1*), tuberculosis

Tuberculosis causes around 1.4 million deaths annually and is a leading cause of death due to an infectious disease. According to the 2021 World Health Organization Report, deaths due to TB increased by 0.4 million due to reduced access to TB diagnosis and treatment during the COVID-19 pandemic (1). Thus, there is an urgent need to identify immune pathways that enable early *Mtb* control and can serve as putative therapeutic targets. There are 13 mammalian PLC isozymes and they are classified into six groups: PLC-β, -γ, -δ,-ε, -ζ, and -η based on their amino acid sequences (2). These isozymes, together with their second messenger 1,4,5-trisphosphate (IP3) and diacylglycerol (DAG), orchestrate a variety of cellular functions, primarily *via* protein kinase-mediated phosphorylation and elevation in intracellular Ca^{2+} levels (3–5). Although all the isoforms share a common core region, their additional binding domains determine their partners and mode of cellular activation (6, 7). *PLC epsilon (PLCε)* has two splice variants *PLCε1* and *PLCε2* and is responsible for catalyzing the hydrolysis of phosphatidylinositol-4,5-bisphosphate (cell membrane phospholipid) to generate IP3 and DAG which are involved in mechanisms such as cell growth, differentiation, and gene expression (8–11). However, among the PLC isoforms, PLCε has a unique role in the signaling pathways that involve small GTPases (6). Its CDC25 domain can act as a guanine nucleotide exchange factor (GEF) for some Ras, GTPase family members (8). Although there is currently a lack

Editor Sabine Ehrt, Weill Cornell Medicine, New York, New York, USA

Address correspondence to Shabaana A. Khader, khader@uchicago.edu.

The authors declare no conflict of interest.

See the funding table on p. 13.

Received 1 December 2023
Accepted 16 February 2024
Published 7 March 2024

of knowledge on the role of PLCε1 in infectious diseases, the role of PLCε in cancer and cardiac diseases is well established (5, 12). For example, polymorphisms in the PLCε gene enhance the risk of acquiring esophageal squamous cell carcinoma and gastric cancer (13, 14). Similar to host-derived PLCε, a bacterial version of PLC from *Mtb* was shown to facilitate the release of DAG from host cell membranes *via* the activation of PKC, MEK/ERK, and NF-κB pathways, resulting in enhanced oxidative stress and eventual cell necrosis (15). Thus, PLC enzymes in general, and PLCε, in particular, might have a role in the host immune responses against *Mtb* infection. Whether host PLCε is expressed in macrophages (16) and contributes to macrophage-mediated inflammatory responses during *Mtb*-infection is unknown.

Differentially expressed genes have been identified in human TB progressors within the well-characterized longitudinal adolescent cohort study (ACS) of South African (SA) patients (17, 18). We identified *PLCƐ1* as a downregulated gene in human and animal TB progressors (18, 19). To address the functional relevance of PLCε1 during TB, we infected *PLCε1*-deficient mice with *Mtb* and found that deficient mice were susceptible to TB. The increased susceptibility was associated with enhanced accumulation of macrophage populations and increased lung proinflammatory cytokine secretion. Macrophages facilitate the primary containment of *Mtb via* their antimicrobial effector functions, including induction of reactive oxygen and nitrogen species. Accordingly, our results show increased *Mtb* burden within *PLCε1*$^{-/-}$ macrophages coincided with significantly reduced nitric oxide production. Together, these results suggest that PLCε1 expression in macrophages is required for mycobactericidal functions and early control of *Mtb* growth.

MATERIALS AND METHODS

Animals

B6 and DO mice were procured from Jackson Laboratory (Bar Harbor, ME) and bred at Washington University in St. Louis. *PLCε1* knockout mouse breeder pair was kindly provided by Prof. Alan Smrcka (University of Michigan) and was bred at Washington University in St. Louis. Mice of both sexes between the ages of 6–8 weeks were used. All mice were maintained and used in accordance with the approved Institutional Animal Care and Use Committee (IACUC) guidelines at Washington University in St. Louis.

Macaque procedures were approved by the Institutional Animal Care and Use Committee of Tulane National Primate Research Center and were performed in accordance with National Institutes of Health (NIH) guidelines. Indian rhesus macaques of both sexes verified to be free of *Mtb* infection by tuberculin skin test were obtained from the Tulane National Primate Research Center. The animals were housed in an ABSL3 facility.

Aerosol infection

Mtb strain HN878 was cultured in Proskauer Beck medium containing 0.05% Tween 80 until reaching the mid-log phase and frozen in 1 mL aliquots at −80 C until used. Mice were aerosol infected with ~100 colony forming units (CFU) and euthanized at decided time points, as described previously (20).

Macaques were exposed to high (~100 CFU) or low (~10 CFU) dose of *Mtb* CDC1551 *via* the aerosol route. The animals were periodically monitored for their physiological parameters and disease symptoms. Macaque progressors were euthanized 5–8 weeks post-challenge and controllers were euthanized 22–24 weeks post-*Mtb* challenge.

Bacterial burden and cytokine analysis

Bacterial burden was assessed using serial 10-fold dilutions of lung or spleen homogenates and plated on 7H11 agar solid medium supplemented with OADC (oleic acid,

bovine albumin, dextrose, and catalase). Colonies were counted after 2–3 weeks of incubation.

Cytokine/chemokine expression was analyzed in lung homogenates from infected mice *via* Luminex (Millipore-Sigma) or ELISA (R&D) as per the manufacturer's protocol.

Generation of single-cell suspensions from tissues and flow cytometry staining

Lung single-cell suspensions from *Mtb*-infected mice were prepared as previously described (21). Briefly, mice were euthanized with CO_2, the right lower lobe was isolated and perfused with heparin in saline. Lungs were minced and incubated with collagenase/DNAse for 30 min at 37°C. Lung tissue was pushed through a 70-µm nylon screen to obtain a single-cell suspension. Following the lysis of erythrocytes, the cells were washed and resuspended in cDMEM (DMEM high glucose + 10% fetal bovine serum + 1% Penicillin/Streptomycin) for flow cytometry staining. For flow cytometric analysis, cells were either stained immediately or stimulated with phorbol myristate acetate (PMA-50 ng/mL) and ionomycin (750 ng/mL; Sigma Aldrich) in the presence of Golgistop (BD Pharmingen).

The following fluorochrome-conjugated antibodies were used for myeloid cell surface staining CD11b APC (clone M1/70), CD11c PeCy7 (Clone HL3, BD Biosciences), GR-1 PerCP-Cy5.5 (Clone RB6-8C5, BD Pharmingen), and MHC class II FITC (Clone M5/114.15.2, Tonbo Biosciences). For myeloid cells, alveolar macrophages were gated as $CD11c^{+}CD11b^{-}$, neutrophils were defined as $CD11b^{+}CD11c^{-}Gr\text{-}1^{hi}$ cells, monocytes were defined as $CD11b^{+}CD11c^{-}Gr\text{-}1^{med}$ cells and recruited macrophages were defined as $CD11b^{+}CD11c^{-}Gr\text{-}1^{low}$ cells. T cells were identified based on the gating strategy shown in supplementary data (Fig. S2A). CD3 AF700 (Clone 500A2, BD Biosciences), CD4 Pacific blue (Clone RM4.5, BD Biosciences), CD44 PeCy7 (Clone 1M7, Tonbo Biosciences), and CD8 APC Cy7 (Clone 53–6.7, BD Biosciences) were used for T-cell surface staining. Fixation/permeabilization buffer (Cat# 554714, BD Bioscience) was used for the intracellular stain to fix and permeabilize lung cells using the manufacturer's protocol. Intracellular staining with IFNγ APC (clone XMG1.2, Tonbo Biosciences) and TNF-α-FITC (Clone MP6-XT22, BD Pharmingen) or the respective isotype control antibodies (APC rat IgG1κ and FITC rat IgG1α isotype, BD Pharmingen) was performed for 30 min. Samples were acquired on a four laser BD Fortessa Flow Cytometer and the analysis was performed using FlowJo (Treestar). The total numbers of cells within each gate were back calculated based on cell counts/individual lung samples.

Histological analysis

The left upper lung lobe was collected for histomorphometric analysis. The lobes were infused with 10% neutral buffered formalin and embedded in paraffin. 5 µm thick lung sections were cut using a microtome, stained with hematoxylin and eosin (H&E), and processed for light microscopy. Formalin-fixed paraffin-embedded (FFPE) lung sections were stained for iNOS (Rabbit anti-mouse/human, Novus Biologicals, Cat#NB300-605SS), CD206 (Goat anti-mouse, R&D systems, Cat# AF2535, RRID:AB_2063012), and F4/80 (Rat anti-mouse, BioRad, Clone Cl:A3-1, Cat#MCA497R, RRID:AB_323279). Images were captured using the automated Nanozoomer digital whole-slide imaging system (Hamamatsu Photonics). Regions of inflammatory cell infiltration were delineated utilizing the NDP view2 software (Hamamatsu Photonics), and the percentage of inflammation was calculated by dividing the inflammatory area by the total area of individual lung lobes. All scoring was conducted in a blinded manner.

Mouse BMDM culture

Bone marrow-derived macrophages (BMDMs) were generated from B6 or *PLCε1*$^{-/-}$ mice. Cells were isolated from the femur and tibia and cultured at 1×10^{6} cells/mL in 10 mL complete DMEM (cDMEM) supplemented with 20 ng/mL of recombinant mouse GM-CSF

(Peprotech, Rocky Hill, NJ, USA) for 3 days at 37°C in 7.5% CO_2, at which point, 10 mL cDMEM supplemented with 20 ng/mL of recombinant mouse GM-CSF was added. Adherent cells (BMDMs) were collected on the seventh day of culture, counted, and plated at 1×10^6 cells/mL in cDMEM.

In vitro infection

BMDMs were infected with *Mtb* HN878 at a multiplicity of infection (MOI) of 1 in a antibiotic-free culture medium. Supernatants from stimulated *in vitro* cultures were collected 6 days post-infection and frozen at −80°C for analysis by enzyme-linked immunosorbent assay and multiplex assay. Infected macrophages were washed rigorously with sterile PBS to remove non-phagocytosed *Mtb*, lysed with 0.05% sterile sodium dodecyl sulfate for 5 min, and then plated in serial dilutions on 7H11 agar plates to estimate intracellular CFU.

Bacterial uptake

In vitro BMDM cultures were infected with HN878-mCherry at an MOI of 1 for 24 hours and 6 days to assess mycobacterial uptake of the reporter *Mtb* HN878. After the removal of the supernatants by centrifugation, infected cells were dislodged from the plate using trypsin and were labeled with fluorochrome-labeled antibodies specific for CD11b (clone M1/70, Tonbo Biosciences). Samples were analyzed for detecting mCherry-positive cells against uninfected controls using the BD FACS Jazz cell sorter and post-run analysis using FlowJo (Tree Star Inc, CA). Data are reported as percentage mCherry-*Mtb* uptake.

RNA sequencing and processing

Human blood RNA-seq data from 46 TB progressors and 107 controls (non-progressors), who participated in the South African ACS, as reported in a previous study (19), were retrieved from the NCBI database. As described by Ahmed et al. (19), mouse or macaque lung tissues were homogenized and snap-frozen in RLT buffer, and DNAse-treated total RNA was extracted using the Qiagen RNeasy Mini kit (Qiagen). RNA sequencing libraries were generated using Clontech SMART-Seq v4 Ultra Low Input RNA Kit for sequencing and Illumina Nextera XT DNA Library preparation kit following the manufacturer's protocol. The cDNA libraries were validated using the KAPA Biosystems primer premix kit with Illumina-compatible DNA primers and quality was examined using Agilent Tapestation 2200. The cDNA libraries were pooled at a final concentration of 1.8 pM. Cluster generation and 75 bp paired-read dual-indexed sequencing were performed on Illumina Next Seq 500. After adapter trimming, RNA-seq reads were aligned to their respective genome assemblies (22) using HISAT2 v2.1.0 (23). FPKM (fragments per kilobase of gene length per million reads mapped) normalization was performed.

Nitric oxide assay

Lung homogenates and BMDM culture supernatants were assessed for levels of nitrite, a stable breakdown product of nitric oxide using the Griess reagent system (Promega) according to the manufacturer's protocol.

Data analysis and statistics

All data were analyzed using the indicated methodology in each figure legend. At least two independent experiments were performed to assure reproducibility. A two sided-unpaired *t*-test (two groups) was performed using GraphPad Prism 5 (La Jolla, CA). Significance is annotated in the figure.

RESULTS

mRNA is downregulated during TB progression across species

We first sought to understand the temporal regulation of *PLCℰ1* gene expression in TB progressors in humans and across animal models of *Mtb* infection. Previously published

transcriptomic data from *Mtb*-infected human as well as animal models led to the identification of *PLCℰ1* as the top DEG downregulated during TB disease progression (18, 19). For further validation, in whole blood transcriptomic data of progressors and controls from the ACS, we found that *PLCℰ1* mRNA expression was downregulated in individuals approximately 6 months prior to active TB disease diagnosis (Fig. 1A). Indeed, *PLCℰ1* expression in lungs of macaque TB progressors and *Mtb*-infected DO mice was measured, similar results were observed (Fig. 1B and C). We further analyzed the timing of induction of PLCε1 protein in the lungs of *Mtb*-infected B6 mice at early and late time points post-challenge. We observed that at early time points [14 days post-infection (dpi)], lungs did not express high levels of PLCε1 or accumulate F4/80$^+$ macrophages. However, by 30 dpi, we observed an increased accumulation of PLCε1$^+$ F4/80$^+$ macrophages which also expressed iNOS. Indeed, accumulation of PLCε1$^+$ macrophages increased at 50 dpi and was stably maintained until 75 dpi (Fig. 1D). Thus, our results show that *PLCℰ1* expression is induced upon exposure to *Mtb* infection in mice and is downregulated with progression toward TB disease.

Mice deficient in signaling are susceptible to early *Mtb* infection

To delineate the functional role of *PLCε1* in *Mtb* infection, we performed in vivo studies in the *PLCε1*$^{-/-}$ mouse model of *Mtb* infection. *PLCε1*$^{-/-}$ and B6 mice were infected with *Mtb* HN878 *via* aerosol route and histopathological and microbiological parameters were studied (Fig. 2A). Mice deficient in the *PLCε1* gene showed enhanced susceptibility and significantly higher lung bacterial burden at 50 and 100 dpi. Mycobacterial dissemination to the spleen was significantly enhanced at 100 dpi in *PLCε1* $^{-/-}$ mice (Fig. 2B). The increased *Mtb* burden in the lung was transient as this increase was not maintained during the later time points assessed (Fig. 2A and B). The increased lung *Mtb* CFU coincided with a significant increase in inflammatory areas in the lungs of *PLCε1*$^{-/-}$ mice as compared to the B6 control (Fig. 2C and D). These results suggest that early PLCε1 expression is required for effective *Mtb* control.

Macrophage accumulation is increased in the lungs of deficient *Mtb*-infected mice

To understand the influence of innate immune cell infiltration, we analyzed the accumulation of myeloid cells in the lungs of B6 and *PLCε1*$^{-/-}$*Mtb*-infected mice. Myeloid populations were identified based on their surface markers. We found a significant increase in the accumulation of MHCII^{hi} alveolar macrophages (AMs) at 50 and 100 dpi in lungs of *PLCε1* $^{-/-}$ *Mtb*-infected mice when compared to B6 *Mtb*-infected mice (Fig. 3A). There were no significant differences in MHCII expression on alveolar macrophages (AMs) based on the similar mean fluorescence intensity (MFI) in the *PLCε1*$^{-/-}$ and B6 mice at all the time points (Fig. 3B). The increased AM numbers remained high until later time points (150 dpi) in the lungs of *PLCε1*$^{-/-}$ mice when compared to B6 *Mtb*-infected lungs. Further analysis of other myeloid cells revealed a significant increase in monocytic infiltration, at both 50 and 100 dpi in the lungs of *PLCε1*$^{-/-}$ post-*Mtb* infection (Fig. 3C). We also observed significant differences in recruited macrophages (RMs) at 100 and 150 dpi (Fig. 3D). In the context of *Mtb* infection and despite the absence of the number of MHCII^{hi} monocytic dendritic cells (mDCs) and neutrophil populations were comparable in the lungs of the *PLCε1*$^{-/-}$ mice and B6 until 100 dpi (Fig. 3E, F, and G) but increased significantly at 150 dpi. The deficiency in PLCε1 therefore contributed to increased accumulation of alveolar macrophages and monocytic cells in the lungs following *Mtb* infection.

We further analyzed the accumulation of T cells in the lungs of *PLCε1*$^{-/-}$*Mtb*-infected mice (gating strategy; Fig. 4A). There was no difference in the number of activated CD4$^+$ CD44^{hi} T cells, in *PLCε1*$^{-/-}$ mice, compared to B6 mice, at all the time points post-*Mtb* challenge (Fig. 4B). TNF-producing CD4$^+$ T cells were significantly decreased only at 100 dpi. However, the numbers were similar at later time points (Fig. 4C). There were

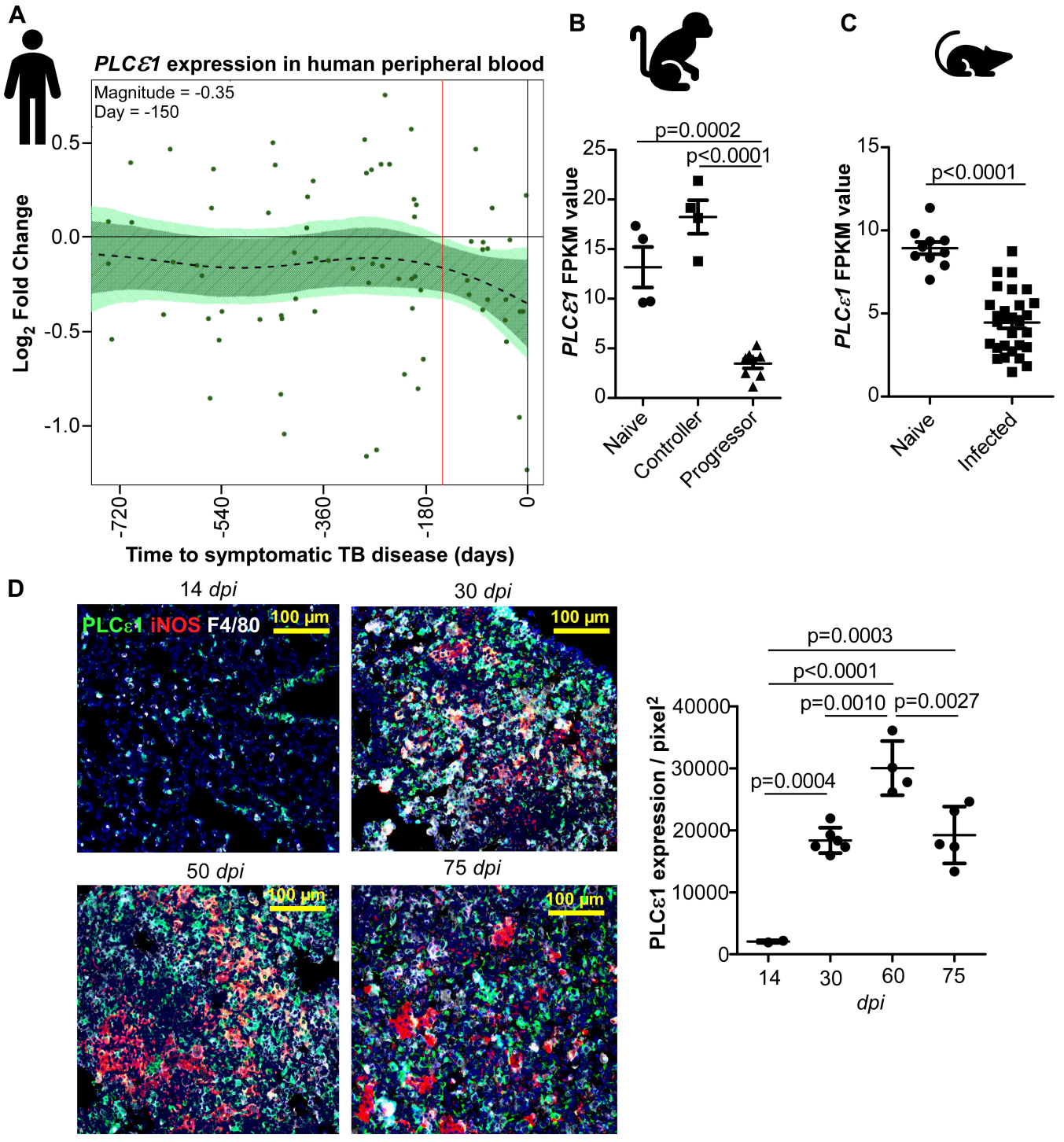

FIG 1 mRNA is downregulated during TB progression across species. mRNA levels of *PLCℰ1* were determined *via* bulk RNA-seq analysis in (A) the Adolescent Cohort Study human blood transcriptomic profile from TB progressors (n = 46) and controllers (n = 107); (B) in the lungs of NHP naïve vs *Mtb*-infected controllers vs progressor macaques (n = 4, 4, and 8, respectively) and (C) in naive (n = 10) and *Mtb* challenged (n = 29) genetically diverse outbred (DO) mice lungs. The expression swarm plots represent false discovery rate-corrected significance values for differential expression calculated by DESeq2. Data represent mean ± SD, with a two-tailed unpaired t-test used to compare between groups. (D) B6 mice lungs were collected at 14, 30, 50, and 75 dpi and stained for PLCε1 (green), iNOS (red), and F4/80 (white). Data represent mean ± SD, one-way ANOVA with Tukey's post-test analysis used to compare between groups.

no differences in the accumulation of lung IFNγ-producing CD4$^+$ T cells between the *Mtb*-infected B6 and *PLCε1*$^{-/-}$ mice at any of the time points (Fig. 4D–G). The results

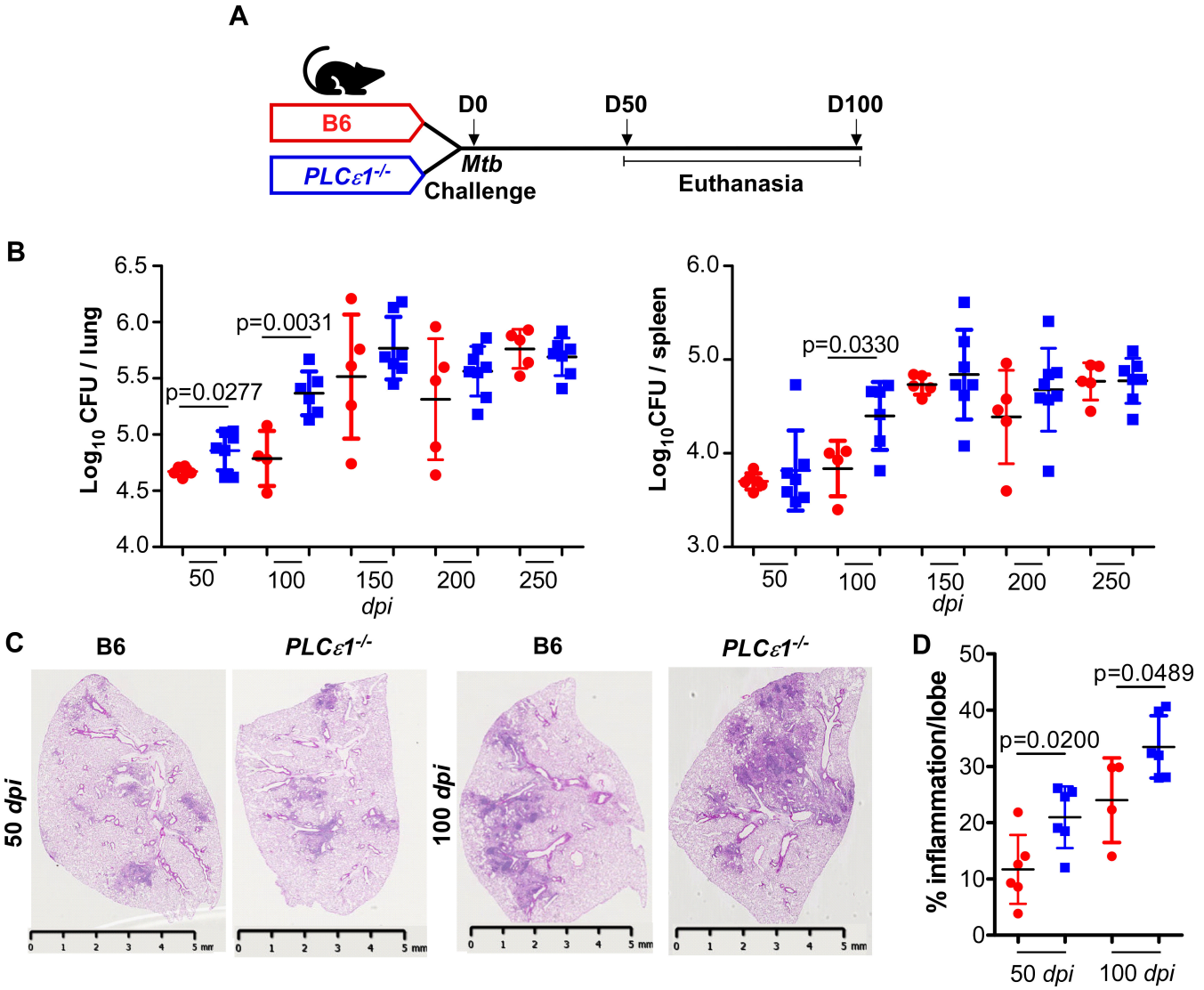

FIG 2 Mice deficient in signaling are more susceptible to *Mtb*. (A) B6 and *PLCε1*$^{-/-}$ mice were infected with *Mtb* HN878, and the lungs were collected and processed at the indicated time points. (B) Lung and spleen *Mtb* burden was enumerated by plating the homogenates on 7H11 agar plates. (C-D) Lung inflammation was analyzed by H&E staining of formalin-fixed paraffin-embedded lung sections; images were taken at 20× magnification and 5 µm scale bar. Data are mean ± SD, with a two-tailed unpaired *t*-test used to compare between groups (n = 4 to 7).

suggest a functional role for signaling in modulating innate but not adaptive immune responses during TB infection.

Macrophage recruiting chemokines are increased in *PLCε1*$^{-/-}$ *Mtb*-infected lungs

To understand the basis of enhanced myeloid cell accumulation at the site of infection, we measured lung chemokines and cytokines in *Mtb*-infected mice. Pulmonary concentrations of monocyte/macrophage recruiting chemokines, monocyte chemoattractant Protein-1 (MCP-1 or CCL2) (24) and macrophage inflammatory protein-1α (MIP-1α or CCL3) (25, 26), were significantly higher in the *Mtb*-infected *PLCε1*$^{-/-}$ mice compared with B6 mice (Fig. 5A). Cytokines that are responsible for differentiation and polarization of monocytes/macrophages such as G-CSF and IL-6 (27) were also increased in the lungs of *Mtb*-infected *PLCε1*$^{-/-}$ mice compared with levels in C57Bl/6 mice at 50 dpi (Fig. 5B). We also found significantly increased levels of KC, a major neutrophil

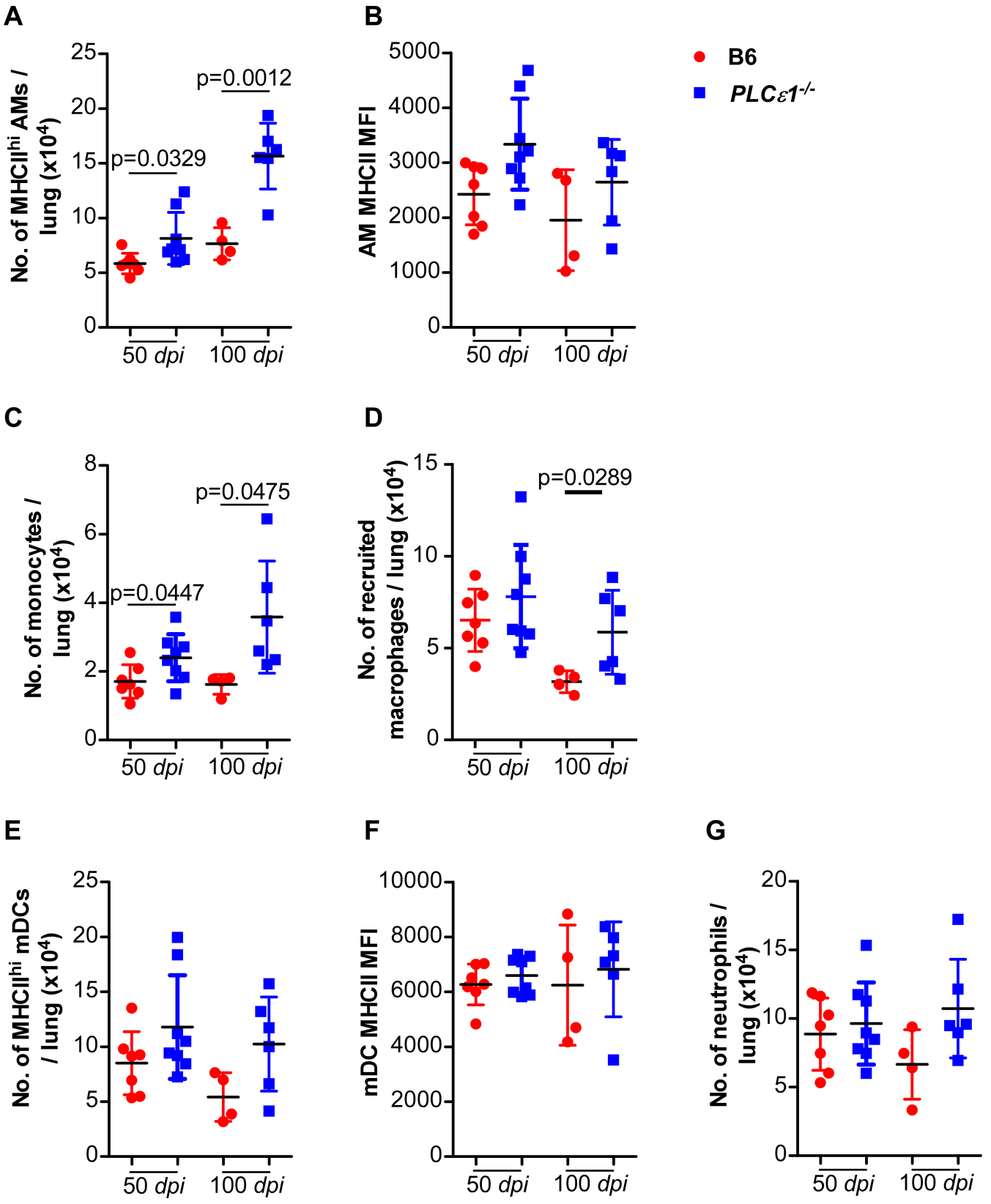

FIG 3 Increased accumulation of lung macrophages in deficient *Mtb*-infected mice. B6 and *PLCε1*$^{-/-}$ (n = 4–8) mice were aerosol infected with ~100 CFU of *Mtb,* at 50 dpi and 100 dpi lungs were analyzed by FACS to determine number of (A) MHCII^{hi} CD11c^{+} alveolar macrophages (AMs), (B) CD11b^{+}Gr1^{int} monocytes, (C) CD11b^{+}Gr1^{lo} recruited macrophages, (D) CD11b^{+} Gr1^{hi} neutrophils, and (E) CD11b^{+} CD11c^{+} monocytic DCs (mDCs). Data represent mean ± SD, with a two-tailed unpaired *t*-test used to compare between groups.

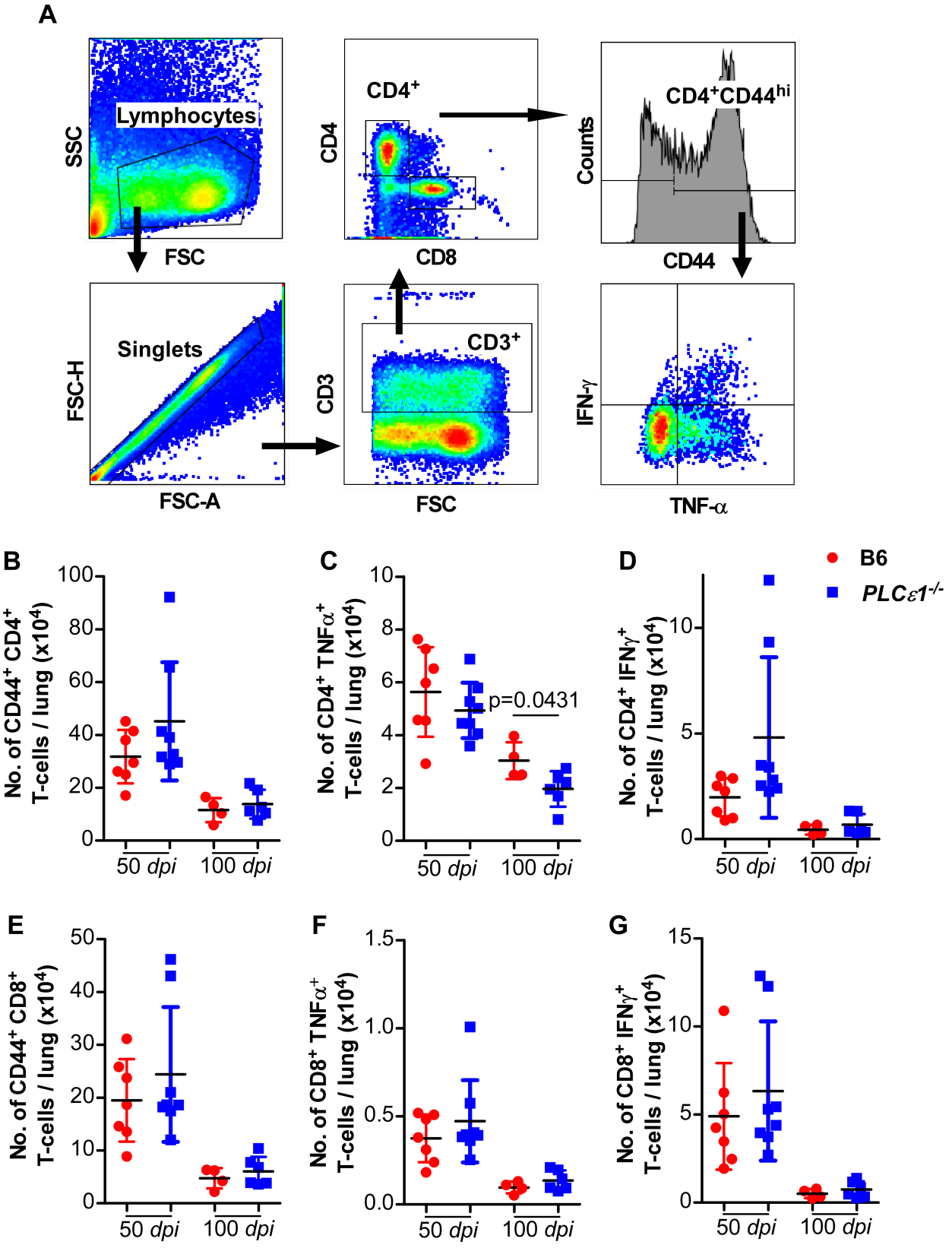

FIG 4 T cells in lungs of deficient mice post-*Mtb* challenge. B6 and *PLCε1*$^{-/-}$ (n = 4–8) mice were aerosol infected with ~100 CFU of *Mtb*, at 50 dpi and 100 dpi lungs were analyzed by FACS to determine number of (A) Gating strategy, number of (B) CD44^{hi}CD4^{+}, (C) activated CD4^{+}TNFα^{+}, (D) activated CD4^{+}IFNγ^{+}, (E) CD44^{hi}CD8^{+}, (F) activated CD8^{+}TNFα^{+}, and (G) CD8^{+}IFNγ^{+}. Data represent mean ± SD, with a two-tailed unpaired t-test used to compare groups.

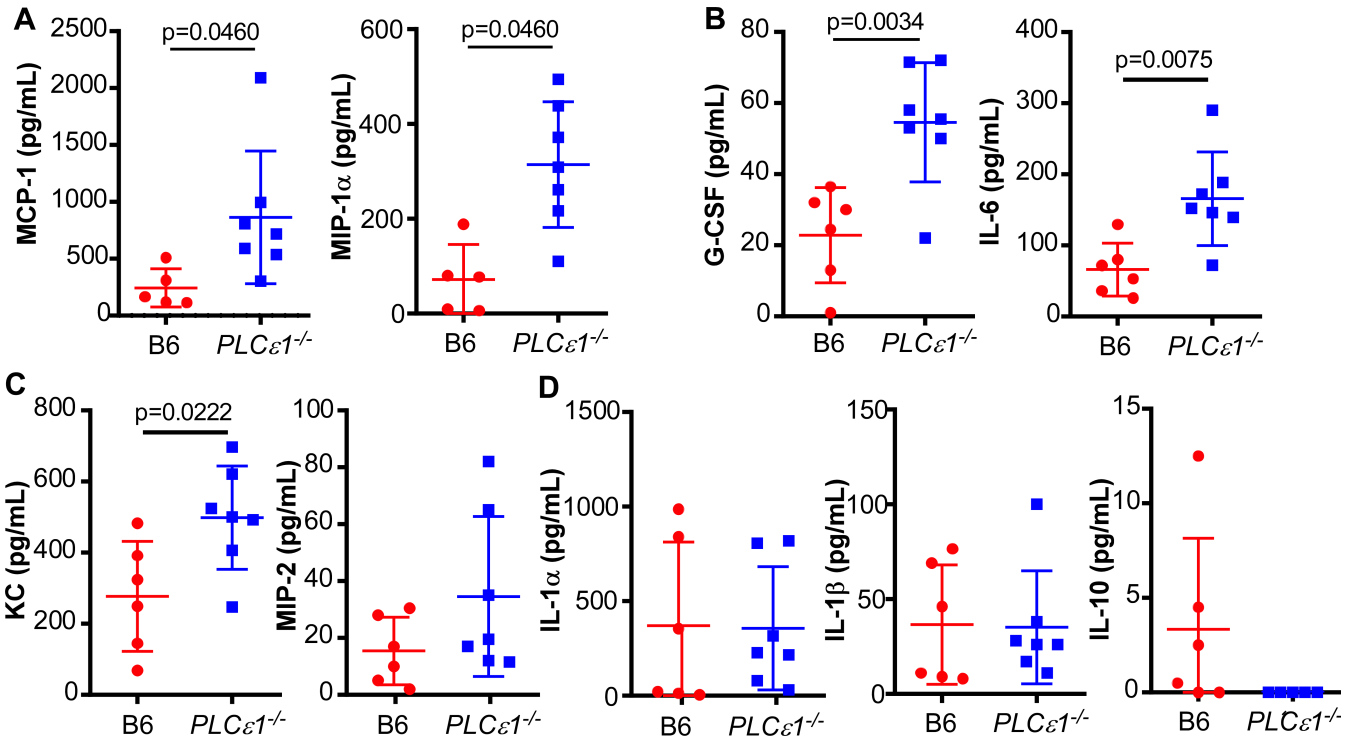

FIG 5 Macrophage recruiting lung chemokines are increased in deficient *Mtb*-infected mice. B6 and *PLCε1*$^{-/-}$ (n = 4–8) mice were aerosol infected with ~100 CFU of *Mtb,* lung lysates were prepared at 50 dpi and analyzed for cytokines specific to (A) monocyte/macrophage recruitment- MCP-1, MIP-1α; (B) macrophage development and activation- G-CSF and IL-6; (C) neutrophil chemoattractant- KC and MIP-2 and (D) pro-inflammatory cytokine IL-α and IL-1β and anti-inflammatory cytokine IL-10. Data represent mean ± SD, with a two-tailed unpaired *t*-test used to compare groups.

chemoattractant (28) in the lungs of *PLCε1*$^{-/-}$ mice compared with B6 mice only at 50 dpi, while there was no difference in macrophage inflammatory protein (MIP-2) levels (Fig. 5C). By contrast, at 100 dpi the chemokines MCP-1 and MIP-1α were significantly reduced in the lungs of *Mtb*-infected *PLCε1*$^{-/-}$ mice compared to B6 mice, whereas factors such as G-CSF, KC, MIP-2, and IL-6 remained unaffected (Fig. S2 A through C). Incidentally, IL-1α and β were found to be similar in the lungs of *Mtb*-infected *PLCε1*$^{-/-}$ mice compared to B6 (Fig. 5D; Fig. S2D). The anti-inflammatory cytokine IL-10, which is produced by both macrophages and activated T cells was similar but at low levels at 50 dpi (Fig. 5D), but was significantly downregulated at 100 dpi (Fig. S2D) in lungs of *PLCε1*$^{-/-}$ mice, compared to B6 mice. Thus, the increased production of chemokine and cytokine profile coincides with increased accumulation of macrophage and monocytes in the lungs of *PLCε1*$^{-/-}$ mice following *Mtb* infection.

PLCε1$^{-/-}$ macrophages display reduced anti-mycobacterial activity

We next hypothesized that the PLC*ε1* gene influences the microbicidal activity of macrophages. Thus, we infected wild-type and *PLCε1*$^{-/-}$ bone marrow-derived macrophages with *Mtb in vitro* (Fig. 6A) and enumerated intracellular *Mtb*. BMDMs from *PLCε1*$^{-/-}$ mice displayed increased uptake of *Mtb* with higher *Mtb* CFU/mL at 6 dpi (Fig. 6B). Indeed, upon infection with a reporter (mCherry) strain of *Mtb* HN878 (Fig. 6A), a higher percentage of *PLCε1*$^{-/-}$ macrophages were infected with mCherry-*Mtb* at 24 hours post-infection (Fig. 6C), suggesting increased bacterial uptake. At 24 hours, the higher mean fluorescent intensity (MFI) of mCherry in the infected *PLCε1*$^{-/-}$ macrophages is suggestive of either increased uptake/replication or also *Mtb* persistence (Fig. 6D).

Nitric oxide (NO) is an effector molecule that macrophages utilize for *Mtb* control. We measured nitrite, as a surrogate of nitric oxide synthase activity, and found it was significantly reduced in *PLCε1*$^{-/-}$ *Mtb*-infected macrophages when compared with B6

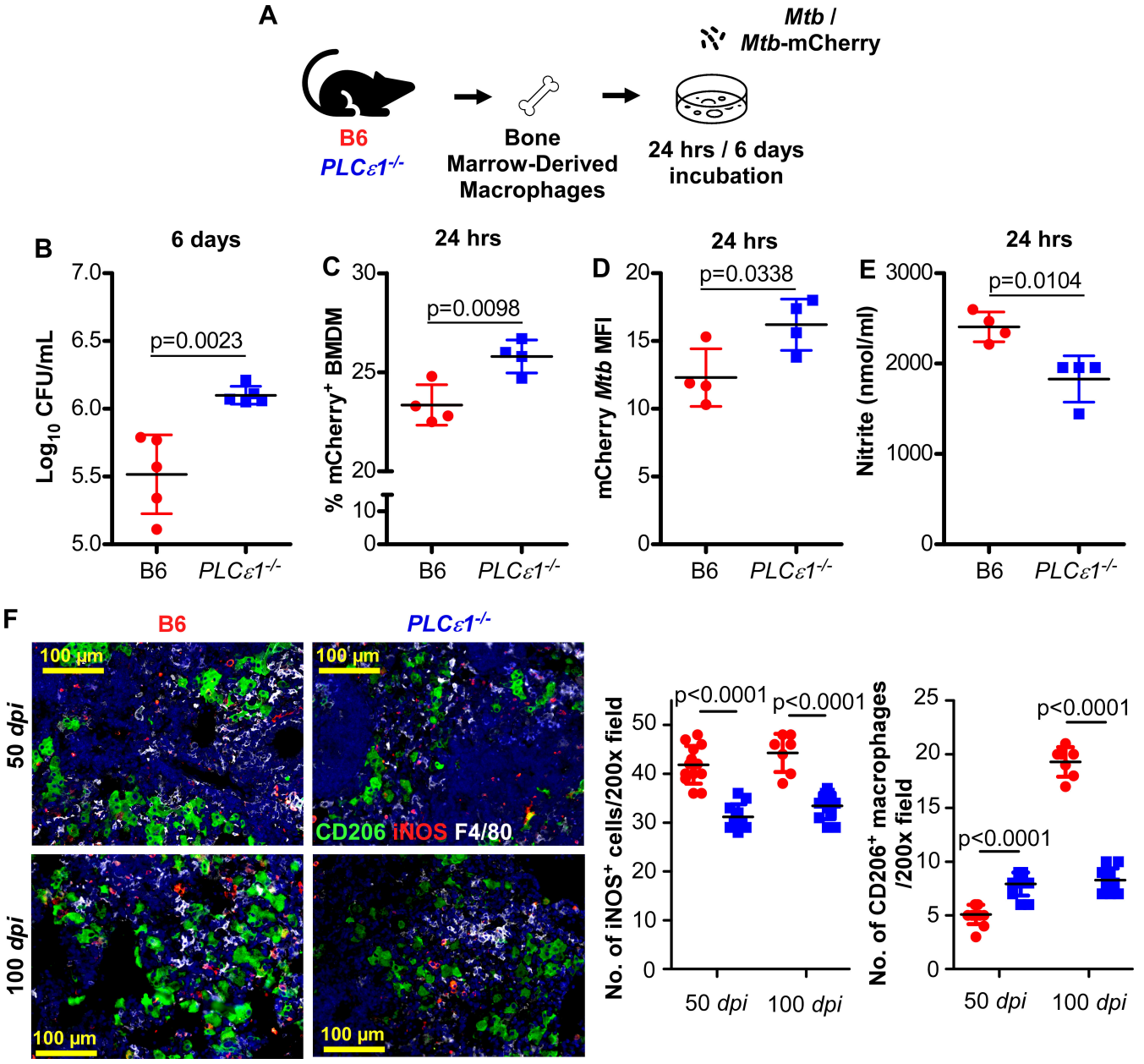

FIG 6 *PLCε1*$^{-/-}$ macrophages display reduced anti-mycobacterial activity. (A) BMDMs prepared from B6 and *PLCε1*$^{-/-}$ mice were either infected with *Mtb* (for 6 days) or with *Mtb* mCherry (for 24 hours) at an MOI of 1; (B) bacterial burden was determined by plating cell lysate on 7H11 agar plates; (C and D) FACS analysis was performed to determine mCherry signal per cell; and (E) nitrate formation was estimated from the supernatant collected 24 hours post-*Mtb* mCherry infection *in vitro*; (n = 4–5). (F–H) Formalin-fixed paraffin-embedded lung sections from *Mtb*-infected mice were obtained at 50 dpi and subjected to IF for iNOS (green), CD206 (red), and F4/80 (white). Data represent mean ± SD, with a two-tailed unpaired *t*-test used to compare groups.

Mtb-infected macrophages (Fig. 6E). These results were consistent with significantly reduced iNOS^{+} cells as well as an increased CD206^{+} M2 macrophages in lungs of *Mtb*-infected *PLCε1*$^{-/-}$ mice lungs at 50 dpi when they show increased bacterial burden (Fig. 6F). Together, these results suggest that signaling plays a role in mediating mycobactericidal effector functions and *Mtb* control via iNOS induction.

DISCUSSION

Macrophages are key players in the innate immune response against *Mtb* infection, where they sense the pathogen, followed by pathogen uptake and activation of downstream signaling pathways within the host cell. PLCℰ1 is an enzyme involved in the generation of secondary messenger IP3 and DAG within all cell types, but its role in macrophage activation during *Mtb* infection is not known. In this study, we investigated the role of *PLCℰ1* during *Mtb* infection. The gene was identified as a possible correlate of risk in TB disease progression in humans (18, 19). Our results confirm that gene expression is downregulated in humans and macaques that progress toward active TB disease when compared to those that control infection. *PLCε1*$^{-/-}$ mouse infected with *Mtb* showed an early defect in *Mtb* control and this coincided with increased lung inflammation. Furthermore, our result highlights the importance of *PLCε1* in regulating macrophage response to *Mtb; PLCε1* in mouse macrophages is required for activation of anti-mycobactericidal activity *via* reactive nitrogen species. Our results using the *PLCε1*$^{-/-}$ mouse model suggest an innate role of in *Mtb* control, through induction of optimal macrophage activation.

PLCε1 is a positive regulator of inflammation in non-immune cells through the induction of cytokines (29) and chemokines *via* activation of the NF-κB pathway (30–34). Here, we report a protective role of *PLCε1* in macrophages. Previous studies underline the integral role of and its second messengers in phagocytosis within leukocytes (35) and the generation of toxic molecules like NO for pathogen clearance (36, 37). Our results showing enhanced bacterial load in *PLCε1*$^{-/-}$ *Mtb*-infected lung and BMDMs suggest a role for PLCε1 in the clearance of intracellular *Mtb*. It could be speculated that the increased *Mtb* burden in *PLCε1*$^{-/-}$ mice in both *in vivo* and in BMDMs is due to the disruption of dependent *Mtb* killing within the host *via* phagosome maturation and subsequent NO production. It is also known that the suppression of phagosome maturation caused by *Mtb* lipids such as trehalose dimycolate (TDM) is overcome by induction of NO in mice (38). Besides the antimicrobial role of NO as part of innate immunity, it can also collaborate with IFNγ to suppress inflammosome-mediated lung tissue damage during the *Mtb* infection (39). While the mechanistic role of NO and iNOS in human macrophage upon TLR activation is non-conclusive (40); there is convincing evidence suggesting upregulation of iNOS expression and increased NO production by peripheral blood monocytes (41), peritoneal (42), and alveolar macrophages (43) upon exposure to *Mtb,* which also correlates with the intracellular bacterial control. Indeed, *Mtb*-infected *PLCε1*$^{-/-}$ lung macrophages had significantly decreased iNOS expression, which was paralleled by significantly decreased NO production by *Mtb*-infected *PLCε1*$^{-/-}$ BMDMs *in vitro*. Thus, together our results highlight a specific role for signaling in optimal macrophage activation during *Mtb* infection; however, the direct involvement of NO remains to be confirmed. Furthermore, it remains to be investigated whether this activation in humans driven by PLCε1 is NO dependent or through a different pathway.

PLCε1 also regulates small GTPase Ras-proximate-1 (Rap1) *via* stromal cell-derived factor 1 alpha (SDF-1α); this signaling is crucial for T-cell adhesion and migration but not cytokine production in delayed-type hypersensitivity (44). Using *PLCε1*-deficient mice, we did not observe any substantial, sustained differences in T-cell numbers or activation; except transient reduction in $CD4^{+}TNF\alpha^{+}$ population in *PLCε1*$^{-/-}$ mice at 100 dpi. It is possible that the presence of *Mtb* causes T-cell infiltration *via* a *PLCε1*-independent mechanism and the increased production of TNF might be an effect of increased *Mtb* load, rather than a direct cause of enhanced susceptibility in our mouse model.

In conclusion, we show a novel role of in host during *Mtb* infection that impacts optimal activation and antimicrobial function of macrophages.

ACKNOWLEDGMENTS

This work was supported by Washington University in St. Louis; NIH grant HL105427, AI111914, AI134236, and AI123780 to S.A.K.; and the Department of Microbiology, University of Chicago.

We thank Dr. Kuldeep S. Chauhan of the Department of Microbiology, University of Chicago, and Ms. Lan Lu of the Department of Molecular Microbiology, Washington University of St. Louis, for technical support and assistance.

S.A.K. supervised all aspects of the study. S.A.K. and A.G. designed the experiments, A.G. performed the experiments, analyzed the data, and constructed figures, and S.A.K. and A.G. wrote the manuscript. S.T., J.R.-M., M.A., D.K., S.K.M., A.S., and T.J.S. performed specific experiments and contributed resources and/or data analysis. S.T., M.A., and R.V.S. contributed to manuscript preparation and editing. S.A.K. provided funding. All authors reviewed, edited, and approved the manuscript.

AUTHOR AFFILIATIONS

[1]Department of Microbiology, The University of Chicago, Chicago, Illinois, USA
[2]Department of Molecular Microbiology, Washington University in St. Louis, St. Louis, Missouri, USA
[3]Division of Allergy, Immunology and Rheumatology, Department of Medicine, University of Rochester Medical Center, Rochester, New York, USA
[4]South African Tuberculosis Vaccine Initiative (SATVI), Institute of Infectious Disease and Molecular Medicine and Division of Immunology, Department of Pathology, University of Cape Town, Cape Town, South Africa
[5]Department of Pharmacology, University of Michigan, Ann Arbor, Michigan, USA
[6]Southwest National Primate Research Centre (SNPRC) at Texas Biomedical Research Institute, San Antonio, Texas, USA

AUTHOR ORCIDs

Ananya Gupta http://orcid.org/0000-0001-7917-7877
Deepak Kaushal http://orcid.org/0000-0003-3521-1257
Shabaana A. Khader http://orcid.org/0000-0002-9545-4982

FUNDING

Funder	Grant(s)	Author(s)
HHS | NIH | OSC | Common Fund (NIH Common Fund)	HL105427, AI111914, AI134236, AI123780	Shabaana A. Khader

AUTHOR CONTRIBUTIONS

Ananya Gupta, Conceptualization, Data curation, Formal analysis, Investigation, Methodology, Software, Validation, Visualization, Writing – original draft, Writing – review and editing | Shyamala Thirunavukkarasu, Formal analysis, Methodology | Javier Rangel-Moreno, Formal analysis, Methodology, Resources | Mushtaq Ahmed, Methodology, Resources | Rosemary V. Swanson, Methodology | Stanley Kimbung Mbandi, Methodology | Alan V. Smrcka, Resources | Deepak Kaushal, Resources | Thomas J. Scriba, Methodology, Resources | Shabaana A. Khader, Conceptualization, Formal analysis, Funding acquisition, Investigation, Resources, Supervision, Validation, Visualization, Writing – review and editing

DATA AVAILABILITY

All bulk RNA-Seq reads are available in NCBI Sequence Read Archive (SRA), Bioproject PRJNA523820.

ADDITIONAL FILES

The following material is available online.

Supplemental Material

Supplemental figures (IAI00495-23-s0001.pdf). Figures S1 and S2.

REFERENCES

1. Global tuberculosis report. 2021, p 25.
2. Gresset A, Sondek J, Harden TK. 2012. The phospholipase C isozymes and their regulation. Subcell Biochem 58:61–94. https://doi.org/10.1007/978-94-007-3012-0_3
3. Rebecchi MJ, Pentyala SN. 2000. Structure, function, and control of phosphoinositide-specific phospholipase C. Physiol Rev 80:1291–1335. https://doi.org/10.1152/physrev.2000.80.4.1291
4. Suh BC, Hille B. 2008. PIP2 is a necessary cofactor for ion channel function: how and why? Annu Rev Biophys 37:175–195. https://doi.org/10.1146/annurev.biophys.37.032807.125859
5. Chandan NR, Smrcka AV, Phan HTN. 2022. Signaling, physiology, and targeting of GPCR -regulated phospholipase C enzymes, p 458–520. In GPCRs as therapeutic targets.
6. Bunney TD, Harris R, Gandarillas NL, Josephs MB, Roe SM, Sorli SC, Paterson HF, Rodrigues-Lima F, Esposito D, Ponting CP, Gierschik P, Pearl LH, Driscoll PC, Katan M. 2006. Structural and mechanistic insights into ras association domains of phospholipase C epsilon. Mol Cell 21:495–507. https://doi.org/10.1016/j.molcel.2006.01.008
7. Dusaban SS, Purcell NH, Rockenstein E, Masliah E, Cho MK, Smrcka AV, Brown JH. 2013. Phospholipase C epsilon links G protein-coupled receptor activation to inflammatory astrocytic responses. Proc Natl Acad Sci U S A 110:3609–3614. https://doi.org/10.1073/pnas.1217355110
8. Bunney TD, Katan M. 2006. Phospholipase C epsilon: linking second messengers and small GTPases. Trends Cell Biol 16:640–648. https://doi.org/10.1016/j.tcb.2006.10.007
9. Rhee SG. 2001. Regulation of phosphoinositide-specific phospholipase C. Annu Rev Biochem 70:281–312. https://doi.org/10.1146/annurev.biochem.70.1.281
10. Song C, Hu CD, Masago M, Kariyai K, Yamawaki-Kataoka Y, Shibatohge M, Wu D, Satoh T, Kataoka T. 2001. Regulation of a novel human phospholipase C, PLCε, through membrane targeting by Ras. J Biol Chem 276:2752–2757. https://doi.org/10.1074/jbc.M008324200
11. Tyutyunnykova A, Telegeev G, Dubrovska A. 2017. The controversial role of phospholipase C epsilon (PLCε) in cancer development and progression. J Cancer 8:716–729. https://doi.org/10.7150/jca.17779
12. Smrcka AV, Brown JH, Holz GG. 2012. Role of phospholipase Cε in physiological phosphoinositide signaling networks. Cell Signal 24:1333–1343. https://doi.org/10.1016/j.cellsig.2012.01.009
13. Hu X, Jia J, Yang Z, Chen S, Xue J, Duan S, Yang P, Peng S, Yang L, Yuan L, Bao G. 2021. *PLCE1* polymorphisms are associated with gastric cancer risk: the changes in protein spatial structure may play a potential role. Front Genet 12:714915. https://doi.org/10.3389/fgene.2021.714915
14. Wang Q, Chen P, Chen D, Liu F, Pan W. 2014. Association between phospholipase C epsilon gene (*PLCE1*) polymorphism and colorectal cancer risk in a Chinese population. J Int Med Res 42:270–281. https://doi.org/10.1177/0300060513492484
15. Assis PA, Espíndola MS, Paula-Silva FWG, Rios WM, Pereira PAT, Leão SC, Silva CL, Faccioli LH. 2014. *Mycobacterium tuberculosis* expressing phospholipase C subverts PGE_2 synthesis and induces necrosis in alveolar macrophages. BMC Microbiol 14:128. https://doi.org/10.1186/1471-2180-14-128
16. Zhu L, Jones C, Zhang G. 2018. The role of phospholipase C signaling in macrophage-mediated inflammatory response. J Immunol Res 2018:5201759. https://doi.org/10.1155/2018/5201759
17. Scriba TJ, Penn-Nicholson A, Shankar S, Hraha T, Thompson EG, Sterling D, Nemes E, Darboe F, Suliman S, Amon LM, Mahomed H, Erasmus M, Whatney W, Johnson JL, Boom WH, Hatherill M, Valvo J, De Groote MA, Ochsner UA, Aderem A, Hanekom WA, Zak DE, other members of the ACS cohort study team. 2017. Sequential inflammatory processes define human progression from *M. tuberculosis* infection to tuberculosis disease. PLoS Pathog 13:e1006687. https://doi.org/10.1371/journal.ppat.1006687
18. Zak DE, Penn-Nicholson A, Scriba TJ, Thompson E, Suliman S, Amon LM, Mahomed H, Erasmus M, Whatney W, Hussey GD, et al. 2016. A blood RNA signature for tuberculosis disease risk: a prospective cohort study. Lancet 387:2312–2322. https://doi.org/10.1016/S0140-6736(15)01316-1
19. Ahmed M, Thirunavukkarasu S, Rosa BA, Thomas KA, Das S, Rangel-Moreno J, Lu L, Mehra S, Mbandi SK, Thackray LB, Diamond MS, Murphy KM, Means T, Martin J, Kaushal D, Scriba TJ, Mitreva M, Khader SA. 2020. Immune correlates of tuberculosis disease and risk translate across species. Sci Transl Med 12:eaay0233. https://doi.org/10.1126/scitranslmed.aay0233
20. Khader SA, Bell GK, Pearl JE, Fountain JJ, Rangel-Moreno J, Cilley GE, Shen F, Eaton SM, Gaffen SL, Swain SL, Locksley RM, Haynes L, Randall TD, Cooper AM. 2007. IL-23 and IL-17 in the establishment of protective pulmonary CD4+ T cell responses after vaccination and during *Mycobacterium tuberculosis* challenge. Nat Immunol 8:369–377. https://doi.org/10.1038/ni1449
21. Gopal R, Rangel-Moreno J, Slight S, Lin Y, Nawar HF, Fallert Junecko BA, Reinhart TA, Kolls J, Randall TD, Connell TD, Khader SA. 2013. Interleukin-17-dependent CXCL13 mediates mucosal vaccine-induced immunity against tuberculosis. Mucosal Immunol 6:972–984. https://doi.org/10.1038/mi.2012.135
22. Zerbino DR, Achuthan P, Akanni W, Amode MR, Barrell D, Bhai J, Billis K, Cummins C, Gall A, Girón CG, et al. 2018. Ensembl 2018. Nucleic Acids Res 46:D754–D761. https://doi.org/10.1093/nar/gkx1098
23. Kim D, Langmead B, Salzberg SL. 2015. HISAT: a fast spliced aligner with low memory requirements. Nat Methods 12:357–360. https://doi.org/10.1038/nmeth.3317
24. Yoshimura T, Robinson EA, Tanaka S, Appella E, Leonard EJ. 1989. Purification and amino acid analysis of two human monocyte chemoattractants produced by phytohemagglutinin-stimulated human blood mononuclear leukocytes. J Immunol 142:1956–1962.
25. Petray P, Corral R, Meckert PC, Laguens R. 2002. Role of macrophage inflammatory protein-1α (MIP-1α) in macrophage homing in the spleen and heart pathology during experimental infection with *Trypanosoma cruzi*. Acta Trop 83:205–211. https://doi.org/10.1016/s0001--706x(02)00131-6
26. Gibaldi D, Vilar-Pereira G, Pereira IR, Silva AA, Barrios LC, Ramos IP, Mata Dos Santos HA, Gazzinelli R, Lannes-Vieira J. 2020. CCL3/macrophage inflammatory protein-1α is dually involved in parasite persistence and induction of a TNF- and IFNγ-enriched inflammatory milieu in *Trypanosoma cruzi*-induced chronic cardiomyopathy. Front Immunol 11:306. https://doi.org/10.3389/fimmu.2020.00306
27. Chomarat P, Banchereau J, Davoust J, Palucka AK. 2000. IL-6 switches the differentiation of monocytes from dendritic cells to macrophages. Nat Immunol 1:510–514. https://doi.org/10.1038/82763
28. De Filippo K, Henderson RB, Laschinger M, Hogg N. 2008. Neutrophil chemokines KC and macrophage-inflammatory protein-2 are newly synthesized by tissue macrophages using distinct TLR signaling pathways. J Immunol 180:4308–4315. https://doi.org/10.4049/jimmunol.180.6.4308
29. Ikuta S, Edamatsu H, Li M, Hu L, Kataoka T. 2008. Crucial role of phospholipase C epsilon in skin inflammation induced by tumor-promoting phorbol ester. Cancer Res 68:64–72. https://doi.org/10.1158/0008-5472.CAN-07-3245
30. Harada Y, Edamatsu H, Kataoka T. 2011. PLCε cooperates with the NF-κB pathway to augment TNFα-stimulated CCL2/MCP1 expression in human keratinocyte. Biochem Biophys Res Commun 414:106–111. https://doi.org/10.1016/j.bbrc.2011.09.032

31. Dusaban SS, Brown JH. 2015. PLCε mediated sustained signaling pathways. Adv Biol Regul 57:17–23. https://doi.org/10.1016/j.jbior.2014.09.014
32. Nagano T, Edamatsu H, Kobayashi K, Takenaka N, Yamamoto M, Sasaki N, Nishimura Y, Kataoka T. 2014. Phospholipase cε, an effector of ras and rap small GTPases, is required for airway inflammatory response in a mouse model of bronchial asthma. PLoS One 9:e108373. https://doi.org/10.1371/journal.pone.0108373
33. Yang X, Ou L, Tang M, Wang Y, Wang X, Chen E, Diao J, Wu X, Luo C. 2015. Knockdown of PLCε inhibits inflammatory cytokine release via STAT3 phosphorylation in human bladder cancer cells. Tumour Biol 36:9723–9732. https://doi.org/10.1007/s13277-015-3712-8
34. Oka M, Edamatsu H, Kunisada M, Hu L, Takenaka N, Sakaguchi M, Kataoka T, Nishigori C. 2011. Phospholipase Cε has a crucial role in ultraviolet B-induced neutrophil-associated skin inflammation by regulating the expression of CXCL1/KC. Lab Invest 91:711–718. https://doi.org/10.1038/labinvest.2011.10
35. Lennartz MR. 1999. Phospholipases and phagocytosis: the role of phospholipid-derived second messengers in phagocytosis. Int J Biochem Cell Biol 31:415–430. https://doi.org/10.1016/s1357-2725(98)00108-3
36. Wadsworth SA, Cavender DE, Beers SA, Lalan P, Schafer PH, Malloy EA, Wu W, Fahmy B, Olini GC, Davis JE, Pellegrino-Gensey JL, Wachter MP, Siekierka JJ. 1999. RWJ 67657, a potent, orally active inhibitor of P38 mitogen-activated protein kinase. J Pharmacol Exp Ther 291:680–687.
37. Lee J-W, Kim NH, Kim J-Y, Park J-H, Shin S-Y, Kwon Y-S, Lee HJ, Kim S-S, Chun W. 2013. Aromadendrin inhibits lipopolysaccharide-induced nuclear translocation of NF-κB and phosphorylation of JNK in RAW 264.7 macrophage cells. Biomol Ther (Seoul) 21:216–221. https://doi.org/10.4062/biomolther.2013.023
38. Axelrod S, Oschkinat H, Enders J, Schlegel B, Brinkmann V, Kaufmann SHE, Haas A, Schaible UE. 2008. Delay of phagosome maturation by a mycobacterial lipid is reversed by nitric oxide. Cell Microbiol 10:1530–1545. https://doi.org/10.1111/j.1462-5822.2008.01147.x
39. Mishra BB, Rathinam VAK, Martens GW, Martinot AJ, Kornfeld H, Fitzgerald KA, Sassetti CM. 2013. Nitric oxide controls the immunopathology of tuberculosis by inhibiting NLRP3 inflammasome-dependent processing of IL-1β. Nat Immunol 14:52–60. https://doi.org/10.1038/ni.2474
40. Gilbertson SE, Walter HC, Gardner K, Wren SN, Vahedi G, Weinmann AS. 2022. Topologically associating domains are disrupted by evolutionary genome rearrangements forming species-specific enhancer connections in mice and humans. Cell Rep 39:110769. https://doi.org/10.1016/j.celrep.2022.110769
41. Wang CH, Lin HC, Liu CY, Huang KH, Huang TT, Yu CT, Kuo HP. 2001. Upregulation of inducible nitric oxide synthase and cytokine secretion in peripheral blood monocytes from pulmonary tuberculosis patients. Int J Tuberc Lung Dis 5:283–291.
42. Nathan C, Shiloh MU. 2000. Reactive oxygen and nitrogen intermediates in the relationship between mammalian hosts and microbial pathogens. Proc Natl Acad Sci U S A 97:8841–8848. https://doi.org/10.1073/pnas.97.16.8841
43. Rich EA, Torres M, Sada E, Finegan CK, Hamilton BD, Toossi Z. 1997. *Mycobacterium tuberculosis* (MTB)- stimulated production of nitric oxide by human alveolar macrophages and relationship of nitric oxide production to growth inhibition of MTB. Tuber Lung Dis 78:247–255. https://doi.org/10.1016/s0962-8479(97)90005-8
44. Strazza M, Azoulay-Alfaguter I, Peled M, Smrcka AV, Skolnik EY, Srivastava S, Mor A. 2017. PLCε1 regulates SDF-1α-induced lymphocyte adhesion and migration to sites of inflammation. Proc Natl Acad Sci U S A 114:2693–2698. https://doi.org/10.1073/pnas.1612900114